The Spectral Cell Method for Ultrasonic Guided Wave Propagation Problems

Sascha Duczek, Steffen Liefold, Ulrich Gabbert

7th European Workshop on Structural Health Monitoring
July 8-11, 2014. La Cité, Nantes, France

THE SPECTRAL CELL METHOD FOR ULTRASONIC GUIDED WAVE PROPAGATION PROBLEMS

Sascha Duczek[1], **Steffen Liefold**[1], **Ulrich Gabbert**[1]

[1] *Otto-von-Guericke-University Magdeburg, Universitätsplatz 2, 39106 Magdeburg*

sascha.duczek@ovgu.de

ABSTRACT

In the current paper we present a fast and robust numerical tool for the simulation of ultrasonic guided waves in heterogeneous structures. The proposed approach, the so-called *spectral cell method* (SCM), combines the fundamental ideas of the spectral element method (SEM) with the fictitious domain concept. The SCM accordingly retains the high convergence rates known from high-order finite element methods and circumvents the need for body-fitted discretizations. Mass-lumping techniques being available for the SEM can also be applied for the SCM, which offers benefits when explicit time-integration methods such as the central difference method (CDM) are employed. Due to these properties both memory requirements and computational time can be notably reduced. The SCM therefore paves the way for an efficient simulation of ultrasonic guided waves. In the first part of the paper we introduce the basic principles of high-order finite element methods (for multi-physics applications - piezoelectricity) and the fictitious domain approach to illustrate the behaviour of the proposed method. The second part contains numerical examples showing that the performance of the SCM is comparable to other (established) high-order methods.

KEYWORDS : *Fictitious Domain Method, High-Order Finite Element Methods, Spectral Element Method, Piezoelectricity, Ultrasonic Guided Waves.*

INTRODUCTION

From a numerical point of view the analysis of wave propagation phenomena in heterogeneous materials is still a highly demanding task. Both a very fine spatial and temporal discretization are needed to obtain accurate results [1]. High-order finite element methods (*ho*-FEM) are consequently a promising candidate to reduce the numerical costs (optimal convergence rates [2, 3]) and are therefore employed in the present paper. Conventional *ho*-FEMs still require a geometry-conforming discretization of the physical domain. This, however, constitutes a severe bottleneck in the simulation pipeline [4], since up to 80 % of the overall analysis time are currently needed to generate the discretization for complex models [5]. The primary objective for the development of efficient and fast numerical methods is consequently seen in decreasing the ratio between the discretization effort and the actual analysis time. One possible approach to alleviate the discretization challenge for complex geometries is the recently proposed finite cell method (FCM) [6, 7]. The FCM is a combination of the fictitious domain concept [8, 9] and *ho*-FEMs [2, 3, 10, 11] for the approximation of the unknown field variables with an adaptive integration technique [7] and the weak imposition of unfitted essential boundary conditions [4]. The core idea of this type of methods accordingly consists in the extension of the physical domain of interest beyond its potentially complex boundaries into a larger embedding domain of simple geometry. This allows for the discretization by a simple structured grid (Cartesian grid), which eliminates the need for the time-consuming and error-prone generation of boundary conforming meshes [4]. For a comprehensive review on the FCM and recent developments we refer to an article by Schillinger and Ruess [4] and the references cited therein.

In the context of wave propagation analysis the SEM is commonly employed [12–16]. The popularity of this method is attributed to the availability of simple -lumping algorithms. We, therefore, propose to combine spectral shape functions with the fictitious domain concept resulting in the so-called *spectral cell method* [17–19]. The SCM accordingly simplifies the mesh generation by employing a fictitious domain approach and approximates the unknown field variables with the aid of spectral shape functions. A special interest, however, is seen in numerical methods to diagonalize the mass matrix. As the discretization is not aligned with the physical boundary of the domain the special finite cells (cut cells) contain both a part of the fictitious domain and the physical domain. These cells consequently need a special treatment to achieve a diagonal mass matrix. This problem has been tackled and successfully solved in reference [19]. The benefits of explicit time-integration schemes, such as the central difference method (CDM), can accordingly be fully exploited [19].
This novel method accordingly paves the way for an efficient simulation of structural health monitoring (SHM) structures. Here, lightweight and highly heterogeneous materials are commonly investigated. In this context Lamb waves or in general ultrasonic guided waves are often used to interrogate the structure. SHM is a well-known technology for estimating the location and the severity of flaws in structures before the defect reaches failure level [20–22]. It relies on the use of signals that include very high frequency contents in order to be able to detect small-scale flaws [23]. The suitability of the proposed method for such SHM-systems will be demonstrated in the following sections.
The article is accordingly organized as follows: In Section 1 we briefly recall the fundamentals of *ho*-FEMs (including piezoelectricity) and introduce the fictitious domain concept. In this context, we propose Lagrange shape functions on a Gauß-Lobatto-Legendre (GLL) grid. We provide two numerical examples to illustrated the behaviour of the SCM in Section 2 The first example is a perforated two-dimensional plate. Using this example the accurate geometry approximation is illustrated. The second example features a three-dimensional plate with a conical hole. Here, the ultrasonic guided waves are excited by collocated piezoelectric transducers. Finally, we give the main conclusion in the last part of the paper at hand.

1. Fundamentals of the Spectral Cell Method

In the present section we briefly provide the basic principles of the SCM. We therefore derive the weak form of the governing equations and explain the fictitious domain concept. For the approximation of the unknown field variables shape functions based on Lagrange polynomials through GLL-points are introduced.

1.1 Weak form

The principle of virtual work is the starting point for the derivation of *ho*-FEMs. For general piezoelectric bodies it is given as [24]

$$\int_{\Omega} \delta\mathbf{u}^T \left(\operatorname{div}(\sigma) + \mathbf{f}_b - \rho\ddot{\mathbf{u}}\right) d\Omega + \int_{\Omega} \delta\varphi \left(\operatorname{div}(\mathbf{D}) - q_b\right) d\Omega = 0 \tag{1}$$

where $\mathbf{f}_b$, ρ, q_b are the vector of mechanical body forces, the density and the electric body charge, respectively. σ and $\mathbf{D}$ denote the mechanical stress tensor and the vector of electric displacements, respectively. $\mathbf{u}$ represents the mechanical displacement field, whereas a dot above the variable stands for the derivative with respect to time. The linear constitutive equations of piezoelectricity relate the stresses and electric displacements to the mechanical strain tensor ε and the electric field vector $\mathbf{E}$ as

$$\sigma = \mathbf{C}\varepsilon - \mathbf{e}^T\mathbf{E}, \tag{2}$$

$$\mathbf{D} = \mathbf{e}\varepsilon + \kappa\mathbf{E}. \tag{3}$$

$\mathbf{C}$, $\mathbf{e}$ and κ denote the matrix of elastic material constants, piezoelectric coupling constants and dielectric constants (permittivity). The strain tensor can be expressed using the mechanical displacements $\mathbf{u}$, and the electric field vector is connected to electric potential φ as

$$\varepsilon = \mathbf{L}_u \mathbf{u}, \tag{4}$$

$$\mathbf{E} = -\mathbf{L}_\varphi \varphi, \tag{5}$$

where $\mathbf{L}_u$ and $\mathbf{L}_\varphi$ denote differential operators. We then proceed to discretize the independent variables $\mathbf{u}$ and φ on the finite element level. This allows us to express the field variables within a finite element in terms of shape functions and the elemental degrees-of-freedom.

$$\mathbf{u} = \mathbf{N}_u \mathbf{u}^{(e)}, \tag{6}$$

$$\varphi = \mathbf{N}_\varphi \varphi^{(e)}. \tag{7}$$

Inserting the discretization of the displacement and the test function into the discretized weak form, we obtain the semi-discrete equations of motion for a piezoelectric body

$$\begin{bmatrix} \mathbf{M}_{uu}^{(e)} & \mathbf{0} \\ \mathbf{0} & \mathbf{0} \end{bmatrix} \begin{Bmatrix} \ddot{\mathbf{u}}^{(\mathbf{e})} \\ \ddot{\varphi}^{(e)} \end{Bmatrix} + \begin{bmatrix} \mathbf{K}_{uu}^{(e)} & \mathbf{K}_{u\varphi}^{(e)} \\ \mathbf{K}_{\varphi u}^{(e)} & -\mathbf{K}_{\varphi\varphi}^{(e)} \end{bmatrix} \begin{Bmatrix} \mathbf{u}^{(e)} \\ \varphi^{(e)} \end{Bmatrix} = \begin{Bmatrix} \mathbf{f}_{uu}^{(e)} \\ \mathbf{f}_{\varphi\varphi}^{(e)} \end{Bmatrix}. \tag{8}$$

The symbols are defined as follows:

Element matrix:
$$\mathbf{M}_{uu}^{(e)} = \int_V \rho\, \mathbf{N}_u^T \mathbf{N}_u \, dV, \tag{9}$$

Mechanical element stiffness matrix:
$$\mathbf{K}_{uu}^{(e)} = \int_V \mathbf{B}_u^T \mathbf{C} \mathbf{B}_u \, dV, \tag{10}$$

Piezoelectric element coupling matrix:
$$\mathbf{K}_{u\varphi}^{(e)} = \int_V \mathbf{B}_u^T \mathbf{e}^T \mathbf{B}_\varphi \, dV = \mathbf{K}_{u\varphi}^{(e)T}, \tag{11}$$

Dielectric element stiffness matrix:
$$\mathbf{K}_{\varphi\varphi}^{(e)} = \int_V \mathbf{B}_\varphi^T \kappa \mathbf{B}_\varphi \, dV, \tag{12}$$

External mechanical element force vector:
$$\mathbf{f}_{uu}^{(e)} = \int_V \mathbf{N}_u^T \mathbf{f}_\mathbf{b} \, dV + \int_O \mathbf{N}_u^T \bar{\mathbf{t}} \, dO, \tag{13}$$

Electric element charge vector:
$$\mathbf{f}_{\varphi\varphi}^{(e)} = -\int_V \mathbf{N}_\varphi^T q_b \, dV - \int_O \mathbf{N}_\varphi^T \bar{Q} \, dO. \tag{14}$$

For a detailed review on the development of finite elements with piezoelectric properties we refer the interested reader to [24] and the references cited therein.

1.2 Fictitious domain concept

To solve the weak form given above using the standard FEMs requires a mesh that is aligned to both internal and external boundaries.We can circumvent this necessity, however, by employing a fictitious domain method [4, 6, 7]. To this end, the physical domain Ω is embedded in a fictitious domain Ω_{fict} resulting in the embedding domain Ω_{ed}, cf. Fig. 1.
We now discretize the embedding domain using a mesh by applying rectangular cells (Cartesian grid) which are independent of the original domain. These "finite elements" of the embedding domain do not necessarily fulfill the usual geometric properties of elements for the physical domain Ω, as

they may be intersected by the boundary of Ω. To distinguish them from classical elements, we call them *finite cells*. It is simpler and more advantageous to apply cells which are rectangular quadrilaterals/hexahedrals in two/three dimensions, resulting in a constant Jacobian matrix of the cell-by-cell mapping function. Fig. 2 illustrates the situation for a two-dimensional setting. Since the original, physical domain is embedded in the domain Ω_{ed} with the boundary S_{ed} Eq. (8) has to be recast. We illustrate this procedure, by way of an example, for the mechanical stiffness matrix Eq. (10) and the mechanical load vector Eq. (13) for a single finite cell

$$\mathbf{K}_{uu}^{(c)} = \int_{\Omega_{ed}} \mathbf{B}_u^T \mathbf{C}_{ed} \mathbf{B}_u \, d\Omega \tag{15}$$

$$\mathbf{f}_{uu}^{(c)} = \int_{\Omega_{ed}} \mathbf{N}_u^T \alpha \mathbf{f_b} \, d\Omega + \int_{S_{ed}} \mathbf{N}_u^T \bar{\mathbf{t}} \, dS. \tag{16}$$

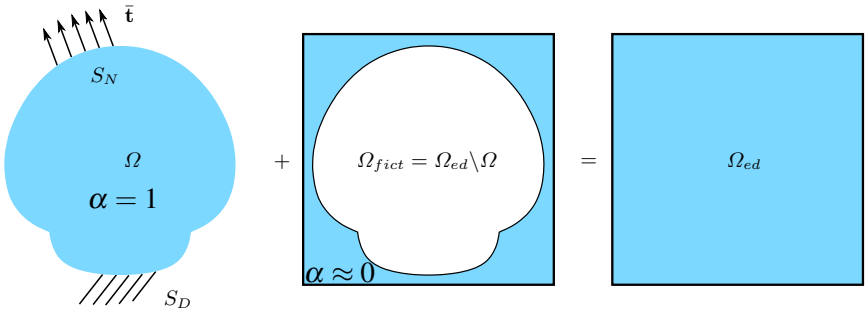

Figure 1 : The physical domain Ω is extended by a so-called fictitious domain Ω_{fict}. This results in a straightforward discretization of the whole embedding domain Ω_{ed}. The influence of the fictitious domain is controlled by the indicator function α.

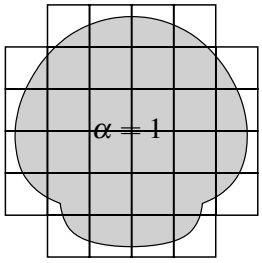

Figure 2 : Finite cell discretization of the embedding domain Ω_{ed}.

The elasticity matrix of the embedding domain $\mathbf{C}_{ed}$ is defined as follows

$$\mathbf{C}_{ed} \quad = \quad \alpha \mathbf{C}. \tag{17}$$

α denotes the so-called indicator function determining whether a point is inside or outside of the physical domain. The indicator function is accordingly defined by

$$\alpha(\mathbf{x}) \quad = \quad \begin{cases} 1.0 & \forall \mathbf{x} \in \Omega \\ 10^{-q} & \forall \mathbf{x} \in \Omega_{ed} \setminus \Omega. \end{cases} \tag{18}$$

The power q is problem-dependent and is typically chosen as $q = 5, \ldots, 10$ [4]. This approach yields in the limit ($q \to \infty$) identical solutions when compared to the finite element method, provided that the geometry is also accurately resolved. In reference [7] an adaptive integration scheme based on a composed Gaussian quadrature rule is proposed. Combined with a space partitioning algorithm this method yields accurate results for the approximation of the geometry [25, 26].

1.3 Shape functions

The presentation of the spectral shape functions is based on the implementation discussed in the monograph by Ostachowicz *et al.* [11]. These p-type elements [27] are based on Lagrange interpolation polynomials defined on a GLL nodal distribution. We define the Gauss-Lobatto points $(\xi_j, \, j = 1, \ldots, (p+1))$ in such a way that

$$\xi_j = \begin{cases} -1 & \text{if} \quad j = 1 \\ \xi_{0,j-1}^{Lo,p-1} & \text{if} \quad 2 \leq j \leq p \\ +1 & \text{if} \quad j = p+1 \end{cases}. \tag{19}$$

Here $\xi_{0,n}^{Lo,p-1}$ $(n=1,\ldots,(p-1))$ denotes the roots of the $(p-1)^{th}$-order Lobatto polynomial

$$Lo_{p-1}(\xi) = \frac{1}{2^p p!}\frac{d^{p+1}}{d\xi^{p+1}}\left[\left(\xi^2-1\right)^p\right]. \tag{20}$$

The basis functions based on Lagrange polynomials are therefore given by

$$N_i^{\text{Lagrange},p}(\xi) = \prod_{j=1,\,j\neq i}^{p+1}\frac{\xi-\xi_j}{\xi_i-\xi_j}, \quad i=1,2,\ldots,p+1. \tag{21}$$

In this case, all degrees-of-freedom retain their physical meaning. If a GLL grid is used in conjunction with the Gauss-Lobatto quadrature, the elemental matrix is under-integrated and diagonalized. This is due to the fact that the integration points coincide with the nodal coordinates. We wish to point out, however, that this set of shape functions is not hierarchical by construction.

2. Numerical Examples

In the present section two numerical benchmark problems are proposed to assess the properties of the SCM in comparison with established tools such as the conventional low-order FEM (h-version of FEM).

2.1 Two-dimensional porous plate

The first example is a porous plate, cf. Fig. 3. The structure is excited by two equal time-dependent forces acting on the left-hand side from opposite directions. This loading facilitates a mono-modal excitation. In the present section the fundamental symmetric mode (S_0) is excited. The plate under consideration is made of aluminum with $E = 70\,\text{GPa}$, $\nu = 0.33$, $\rho = 2700\,\text{kg/m}^3$ and is in a state of plane strain. Symmetry boundary conditions are applied to the left-hand side of the plate, and the plate is excited on the left-hand side in x_2-direction by time-dependent force given by

$$F(t) = \hat{F}\sin(\omega t)\sin^2\left(\frac{\omega t}{2n}\right), \tag{22}$$

where $\hat{F}$ is the amplitude, $\omega = 2\pi f$ denotes the central circular frequency, and n denotes the number of cycles determining the width of the excited frequency band around the central frequency f. In this example, we set $\hat{F} = 0.5\,\text{N}$, $f = 250\,\text{kHz}$ and $n = 5$.

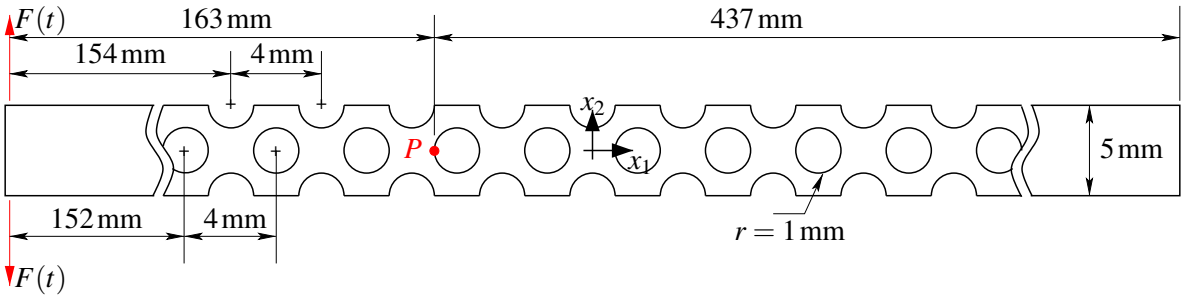

Figure 3 : Porous plate with 13 circular holes in the middle and 12 semi-circular cut-outs on each side (top and bottom edge). The Neumann boundary (excitation forces) conditions are also illustrated. The coordinates of the three measurement points are: P1 ($x_{1P_1} = 100\,\text{mm}$, $x_{2P_1} = 2.5\,\text{mm}$), P2 ($x_{1P_2} = 163\,\text{mm}$, $x_{2P_2} = 0\,\text{mm}$), P3 ($x_{1P_3} = 302\,\text{mm}$, $x_{2P_3} = 2.5\,\text{mm}$) [19].

In the current investigation, the domain of interest is discretized by a Cartesian grid employing 4×400 cells with a polynomial degree of $p = 6$. The time history of the displacements at the point of interest - marked in Fig. 3 - are depicted in Fig. 4. An excellent agreement between the different numerical approaches can be observed. It must be kept in mind that, although the geometry of this example is fairly complex, the generation of meshes using the SCM requires hardly any effort, which can be regarded as the main advantage of an fictitious domain approach. The main advantage of using the SCM instead of the FCM is the diagonal matrix [19]. We lump the matrix of the cells that are entirely filled with material with the aid of the GLL nodal quadrature [13, 14]. For the cut cells, we employ the HRZ-lumping technique as proposed in reference [19, 28].

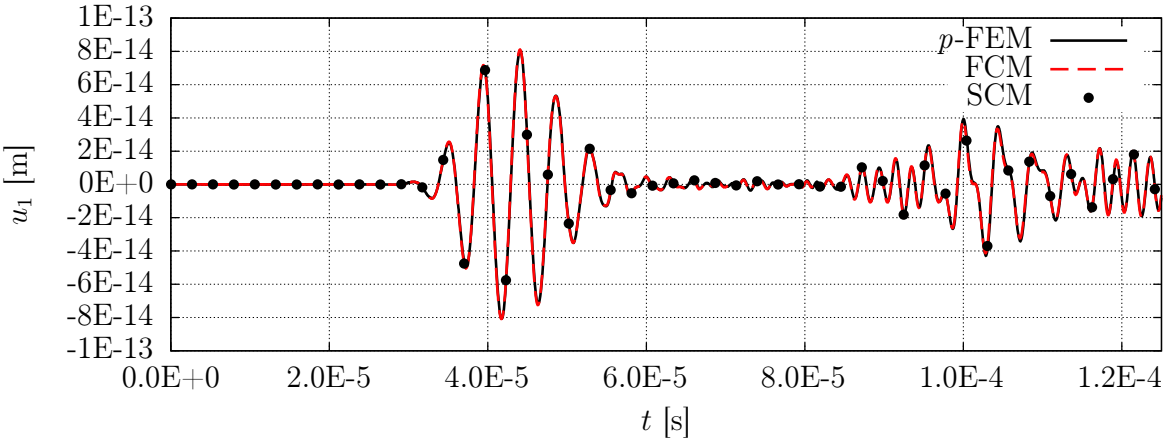

Figure 4 : Comparison of the time history of the displacements for the different numerical.

2.2 Three-dimensional plate with a conical hole

The second example involves the propagation of ultrasonic guided waves in a three-dimensional aluminum plate with a conical through the thickness hole, cf. Fig 5. The ultrasonic waves are excited using collocated piezoelectric actuators. This problem demonstrates important features of guided waves like mode conversion and physical dispersion. The size of the finite cells is chosen according

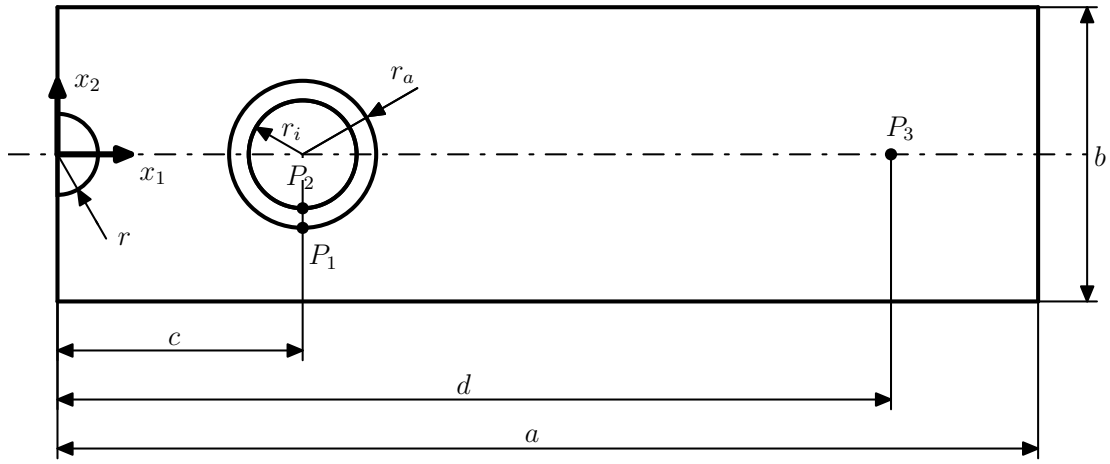

Figure 5 : Aluminum plate with a conical hole. Dimensions: $a = 300\,\text{mm}$, $b = 200\,\text{mm}$, $c = 50\,\text{mm}$, $d = 200\,\text{mm}$, $r_a = 10\,\text{mm}$, $r_i = 9\,\text{mm}$, $h = 2\,\text{mm}$ (thickness of the plate). The piezoelectric transducers are made of PIC-151.

to the guidelines proposed by Willberg *et al.* [1]. The spectral cell model uses an anisotropic ansatz

space, meaning that different polynomial degrees are chosen in out-of-plane and in in-plane direction. The in-plane polynomial degrees are accordingly $p_{x_1} = p_{x_2} = 3$ and the out-of-plane polynomial order is $p_{x_3} = 4$. To ensure accurate results, the element/cell size is $b_e = 0.2828\,\text{mm}$.
Since no analytical solution is available for this benchmark problem, we compare the results of the different high-order FE-approaches with an ABAQUS reference solution deploying 20-node hexahedral finite elements (C3D20) on a very fine grid ($n_{dof} \approx 1.5 \cdot 10^6$). This corresponds to more than 50 nodes per wavelength to ensure a converged solution with high accuracy. Please note that the symmetry of the structure is exploited to save numerical effort, so the model only depicts half of the plate. Fig. 6 displays the time history of the displacements at point P_2.
The agreement between the proposed high-order fictitious domain methods and the commercial software ABAQUS is remarkable. The relative error in group velocity between the reference solution and the introduced methods is less than 0.1%. We consequently conclude that the finite and spectral cell methods are able to capture and resolve characteristic features of ultrasonic guided-wave propagation. Please refer to [18, 19] for a thorough assessment of the convergence properties of the SCM. In these articles it is shown that the computational time can be significantly reduced by achieving a similar accuracy of the simulation results.

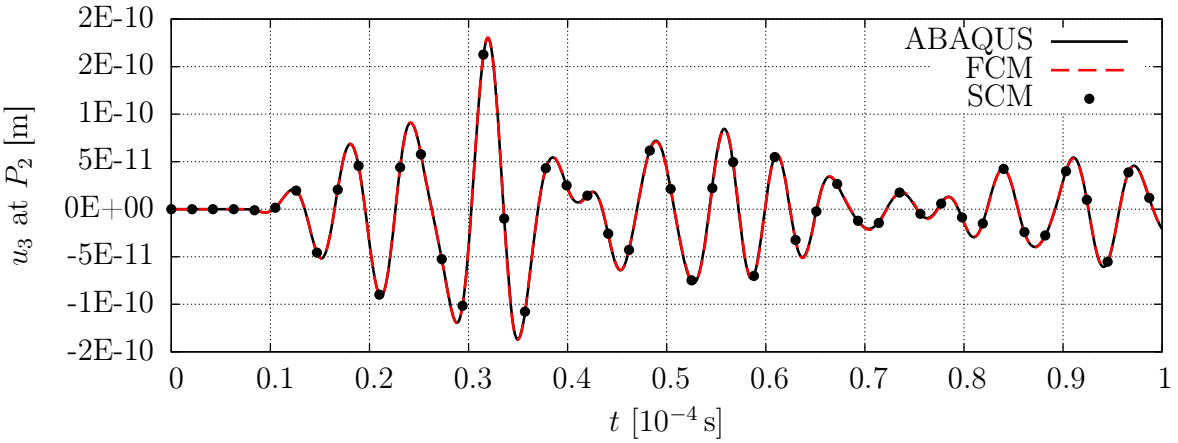

Figure 6 : Comparison of the ABAQUS reference solution at point P_2 to the FCM/SCM results, obtained using the optimal discretization as proposed in [1].

CONCLUSION

The SCM is a fast discretization technique which makes it possible to model structures with complicated geometries with very reasonable computational input. It paves the way for exploiting the advantages of explicit time-integration schemes. In the SCM the mass matrix of the cells that are completely within the physical domain are by definition diagonal. For cut cells, however, a mass-lumping technique based on the HRZ-technique can be employed. The resulting method shows high convergence rates and decreases the computational time by at least one order of magnitude compared to implicit solvers such as the Newmark method [18, 19]. The spectral cell method is therefore an appropriate candidate for wave propagation analysis involving complicated geometries.

REFERENCES

[1] C. Willberg, S. Duczek, J. M. Vivar-Perez, D. Schmicker, and U. Gabbert. Comparison of different higher order finite element schemes for the simulation of Lamb waves. *Computer Methods in Applied Mechanics and Engineering*, 241-244:246–261, 2012.

[2] B. Szabó and I. Babuška. *Finite Element Analysis*. John Wiley and Sons, 1991.

[3] B. Szabó and I. Babuška. *Introduction to Finite Element Analysis: Formulation, Verification and Validation*. John Wiley and Sons, 2011.

[4] D. Schillinger and M. Ruess. The finite cell method: A review in the context of high-order structural analysis of CAD and image-based geometric models. *Acta Mechanica*, submitted:64pp., 2014.

[5] J. A. Cottrell, T. J. R. Hughes, and Y. Bazilevs. *Isogeometric Analysis: Toward Integration of CAD and FEA*. John Wiley & Sons, 2009.

[6] J. Parvizian, A. Düster, and E: Rank. Finite cell method: *h*- and *p*-extension for embedded domain problems in solid mechanics. *Computational Mechanics*, 41:121–133, 2007.

[7] A. Düster, J. Parvizian, Z. Yang, and E: Rank. The finite cell method for three-dimensional problems of solid mechanics. *Computer Methods in Applied Mechanics and Engineering*, 197:3768–3782, 2008.

[8] C. S. Peskin. The fluid dynamics of heart valves: Experimental, theoretical and computational methods. *Annual Review of Fluid Mechanics*, 14:235–259, 1981.

[9] I. Ramière, P. Angot, and M. Belliard. A fictitious domain approach with spread interface for elliptic problems with general boundary conditions. 196:766–781, 2007.

[10] A. T. Patera. A spectral element method for fluid dynamics: Laminar flow in a channel expansion. *Journal of Computational Physics*, 54:468–488, 1984.

[11] W. Ostachowicz, P. Kudela, M. Krawczuk, and A. Żak. *Guided Waves in Structures for SHM: The Time-Domain Spectral Element Method*. John Wiley & Sons, 2011.

[12] D. Komatitsch, D. Michéa, and G. Erlebacher. Porting a high-order finite-element earthquake modeling application to NVIDIA graphics cards using CUDA. *Journal of Parallel and Distributed Computing*, 69:451–460, 2009.

[13] D. Komatitsch and J. Tromp. Spectral-element simulations of global seismic wave propagation I. - Validation. *International Journal of Geophysics*, 149:390–412, 2002.

[14] D. Komatitsch and J. Tromp. Spectral-element simulations of global seismic wave propagation II. - Three-dimensional models, oceans, rotation and self-gravitation. *International Journal of Geophysics*, 150:303–318, 2002.

[15] P. Kudela and W. Ostachowicz. 3d time-domain spectral elements for stress waves modelling. *Journal of Physics: Conference Series*, 181:1–8, 2009.

[16] K. Lonkar and F.-K. Chang. Modeling of piezo-induced ultrasonic wave propagation in composite structures using layered solid spectral element. *Structural Health Monitoring*, 13:50–67, 2014.

[17] S. Duczek, M. Joulaian, A. Düster, and U. Gabbert. Modeling of ultrasonic guided waves using the finite cell method. In *SPIE Smart Structures and Materials + Nondestructive Evaluation and Health Monitoring, vol. 86951U, International Society for Optics and Photonics*, 2013.

[18] S. Duczek, M. Joulaian, A. Düster, and U. Gabbert. Numerical analysis of Lamb waves using the finite and spectral cell method. *International Journal for Numerical Methods in Engineering*, accepted:pre–print, 2014.

[19] M. Joulaian, S. Duczek, U. Gabbert, and A. Düster. Finite and spectral cell method for wave propagation in heterogeneous materials. *Computational Mechanics*, accepted:pre–print, 2014.

[20] W. J. Staszewski. *Health Monitoring for Aerospace Structures*. John Wiley & Sons, 2003.

[21] C. Boller. *Encyclopedia of Strcutural Health Monitoring*. John Wiley & Sons, 2009.

[22] S. Gopalakrishnan, M. Ruzzene, and S. Hanagud. *Computational Techniques for Structural Health Monitoring*. Springer, London, 2011.

[23] J. Pohl, C. Willberg, U. Gabbert, and G. Mook. Experimental and theoretical analysis of Lamb wave generation by piezoceramic actuators for structural health monitoring. *Experimental Mechanics*, 52:429–438, 2012.

[24] A. Benjeddou. Advances in piezoelectric finite element modeling of adaptive structural elements: A survey. *Computers & Structures*, 76:347–363, 2000.

[25] A. Abedian, J. Parvizian, A. Düster, H. Khademyzadeh, and E. Rank. Performance of different integration schemes in facing discontinuities in the finite cell method. *International Journal of Computational Methods*, 10:24pp., 2013.

[26] A. Abedian, J. Parvizian, A. Düster, and E. Rank. The finite cell method for the J_2 flow theory of plasticity. *Finite Elements in Analysis and Design*, 69:37–47, July 2013.

[27] L. L. Thompson and P. M. Pinsky. Complex wavenumber Fourier analysis of the *p*-version finite element method. *Computational Mechanics*, 13:255–275, 1994.

[28] E. Hinton, T. Rock, and O. C. Zienkiewicz. A note on mass lumping and related processes in the finite element method. *Earthquake Engineering and Structural Dynamics*, 4:245–249, 1976.